ORIGINAL ARTICLE

Modeling of machining distortion for thin-walled components based on the internal stress field evolution

Yuan Ma[1] · Jianfu Zhang[2] · Dingwen Yu[2] · Pingfa Feng[1,2] · Chao Xu[1]

Abstract

Machining distortion is a major issue in the machining of thin-walled monolithic components, which are now widely used in the aerospace industry. The evolution of the stress field within the workpiece during machining (due to material removal and cutting loads) is the main cause of global machining distortion for thin-walled parts. This paper presents a new modeling method for machining distortion that can represent this stress evolution process. The finite element method (FEM) is used to model the material removal and mechanical loads during roughing. Theoretical modeling is used to model the influence of finishing on stress redistribution within surface material. Finally, FEM is used to calculate the machining distortion. This method can be implemented on small servers and personal computers. An application case of a thin-walled component was considered. The simulation result with the new method showed superior accuracy compared with traditional simulation method. The method presented could be used to predict the machining distortion for parts, which would allow further improvement in machining techniques.

Keywords Residual stress · Evolution process · Machining distortion · Aerospace monolithic component · Thin-walled structure

1 Introduction

Monolithic components made of large-scale workblanks are now widely used in modern airplanes. However, overcoming the machining distortion of these thin-walled components has become one of toughest challenges for aviation industry [1].

The relaxation, or redistribution, of the residual stress within the workblank (due to the hot working and cold working processes) is regarded as one of the most important causes of machining distortion [2, 3]. The removal of material breaks the initial self-equilibrating state of the internal stress field. The redistribution of internal stress causes distortion. Garcia et al. [4] studied the characteristics of machining distortion caused by quenching residual stress. Wang [5] systematically studied the formation and relief mechanism of the initial stress within aluminum alloy plates. Robinson et al. [6] measured and simulated the redistribution of residual stress and the distortion caused by material removal. Machining is not just a material removal process, it also involves cutting loads. Guo [7], and Rai and Xirouchakis [8], built relatively comprehensive finite element models to predict the machining distortion, which considered tool path and added cutting loads on the elements along with element killing operation. Furthermore, machining is more than just a material removal process with external loads, it also causes severe plastic deformation. Additionally, it significantly changes the stress distribution within the surface layer. This is known as machining-induced residual stress (MIRS), which can influence the performance of machined parts like fatigue life, corrosion resistance, etc. [9, 10]. MIRS is also a source of machining distortion for thin-walled components [11]. Consequently, MIRS must be accounted for to precisely predict the machining distortion of thin-walled components. Young [12] used Legendre polynomials to represent the distribution of MIRS for the prediction of machining distortion in thin-walled parts. Huang [13] used MIRS distribution (measured from one position) to simulate the machining distortion. It is a simplification to assume that the distribution of MIRS is the same at all machined surfaces. In fact, the residual stress would not be uniform because of different machining parameters and the non-uniform initial residual stress [14].

✉ Jianfu Zhang
zhjf@tsinghua.edu.cn

1 Division of Advanced Manufacturing, Graduate School at Shenzhen, Tsinghua University, Energy and Environment Building, University Town, Shenzhen 518055, Guangdong, China

2 State Key Laboratory of Tribology, Department of Mechanical Engineering, Tsinghua University, Lee Shau Kee Sci. & Tech. Building, Beijing 100084, China

Currently, it is not practical to test the overall residual stress distribution for monolithic components. Progress has been made using FEM analysis for the metal cutting process [15, 16]. However, it is time consuming and computationally expensive. Consequently, it is not applicable for part-level machining simulation. Alternatively, analytical prediction of MIRS is a feasible approach. The main source of MIRS is the non-uniform plastic deformation introduced by thermal and mechanical loads [17]. The theoretical prediction can be achieved by analyzing the stress-strain field caused by the loading and releasing process of cutting loads. Liang and Su [18] proposed a two-dimensional theoretical algorithm for turning residual stress based on rolling/sliding contact theory, mainly considering mechanical loads. Then, Su et al. [19] further consider thermal loads. Huang et al. [20] and Huang et al. [21] optimized the relaxation algorithm for the calculation of residual stress. Fergani et al. [22] modeled the regeneration of residual stress in multi-pass milling. Currently, theoretical models of MIRS are based on many simplifications. However, theoretical models can achieve acceptable accuracy and good efficiency when configured appropriately.

The generation of global machining distortion for thin-walled components (excluding local deflection caused by cutting forces) is determined by the evolution of the internal stress field of the workpiece. This internal stress field is initially introduced by forming and the hot/cold working process. It then evolves gradually during the machining process until reaching a new self-equilibrating state. The internal stress field evolves simultaneously with the strain field, which results in machining distortion. This study proposes a new modeling method of machining distortion based on analysis of the evolution process of the internal stress field. It includes the bulk stress evolution (caused by material removal and cutting loads) and the MIRS within the surface layer.

2 Simulation method of stress evolution and machining distortion

2.1 Simulation strategy for machining process for thin-walled components

The proposed simulation method is shown in Fig. 1. The initial residual stress within the workblank is input. This initial stress can be measured using the crack compliance method [23] for the widely used pre-stretched aluminum alloy plates. The residual stress measured along the thickness direction can

Fig. 1 Simulation strategy for the machining process for aeronautical components
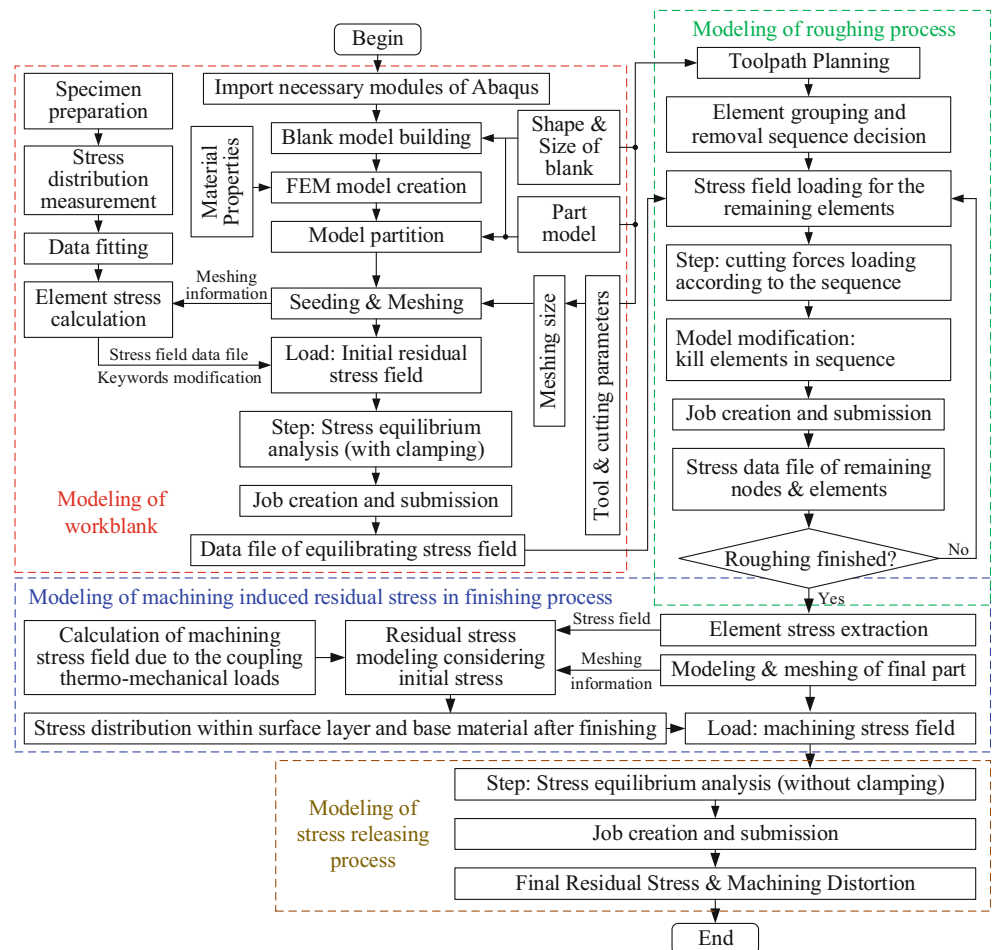
be fitted with polynomials. The initial stress state for each element in the finite element model can be calculated according to its coordinates. A stress equilibrium analysis step is added to achieve the balanced stress distribution. Finite element simulation can be used to obtain the initial stress distribution, especially for forged or casted workblanks [24, 25]. Simulation of the roughing process mainly reproduces the material removal process (which significantly changes the distribution of bulk residual stress), and the mechanical loads (which can be in 10^2–10^3 N and may influence the global stress redistribution). The influence of cutting heat and MIRS is not considered for the roughing process for the following reasons: (1) cutting heat mainly influences the local stress distribution near the cutting area; (2) during the roughing process, the machined surface layer containing MIRS would be removed by later cutting passes; (3) thermomechanical coupling analysis is much more computationally expensive than mechanical analysis in FEM analysis.

The machined surface left by the last finishing pass contains MIRS, the amplitude, and distribution gradient of which are usually larger than that of the residual stress within bulk material. This residual stress field will redistribute after machining when fixtures are removed. This contributes to the machining distortion. Here, a theoretical modeling method is applied. The residual stress field after the roughing process is

used as the initial stress state for the calculation of MIRS after finishing. The stress data is then loaded into the finite element model to calculate the final residual stress and machining distortion (after releasing all the clamps and constraints).

2.2 Simulation method for the roughing process

The roughing process can be represented with an element removal process that follows a particular sequence and undergoes cutting loads, as shown in Fig. 2. The element removal operation can be achieved with the model change function of ABAQUS. Mechanical loads are added on the nodes of elements to be removed in each analysis step. The width of cut (WOC) equal to the tool radius is frequently used in the roughing process. WOC is equal to the diameter of the tool in the entry cutting pass. For convenience, the length and width of elements are suggested to be equal to the tool radius. Cutting loads are added according to the feeding and rotation direction of the tool, as shown in Fig. 3. Figure 3a–d represent different feeding directions in machining where WOC is less than or equal to the tool radius. Figure 3 e–h are for machining where WOC is equal to the tool diameter.

The FEM model built for roughing simulation is referred to as the roughing model (RM). The following operations are performed on the RM: (1) loading of initial residual stress in

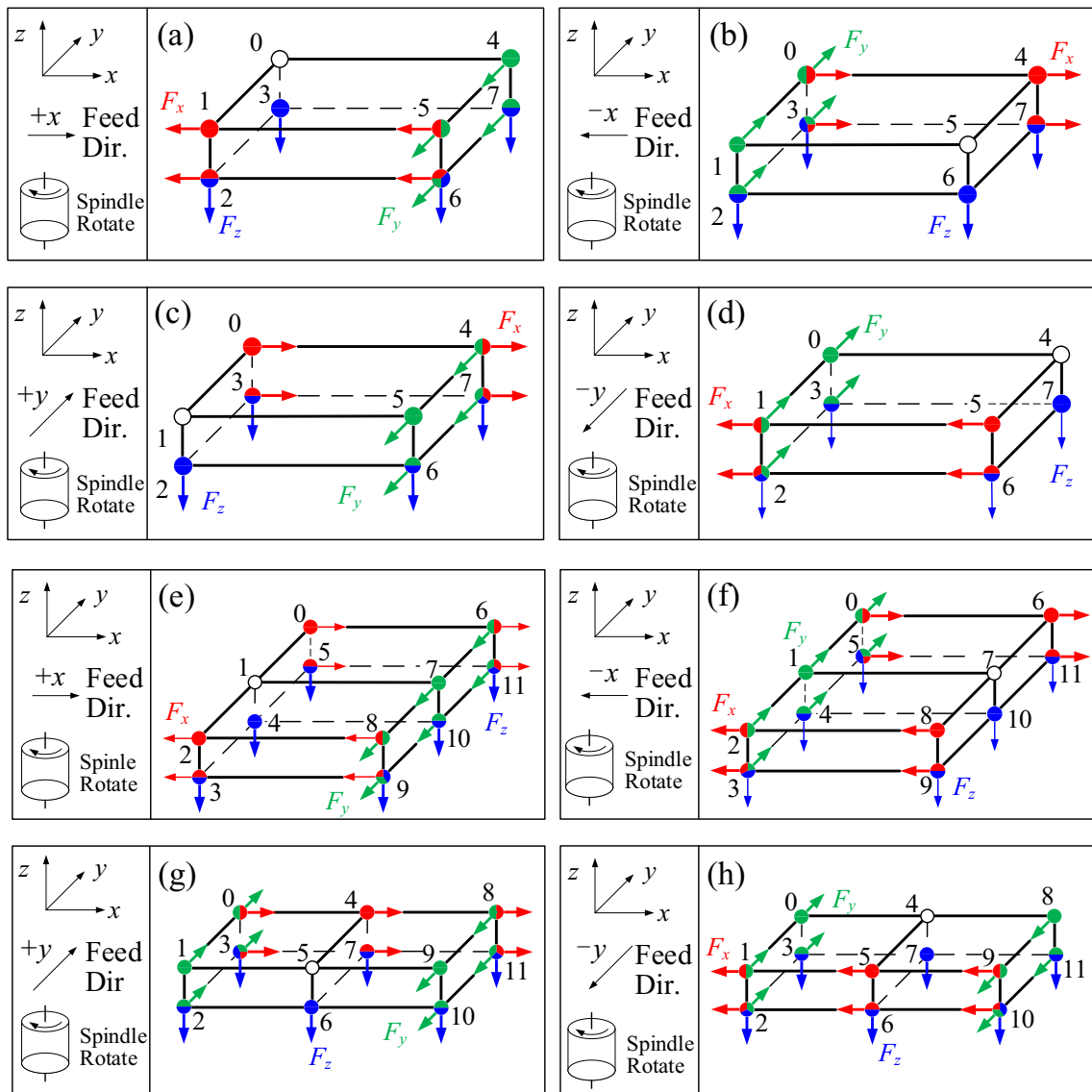Fig. 2 Simplified simulation method of the roughing process

Simplified mesh model for roughing simulation
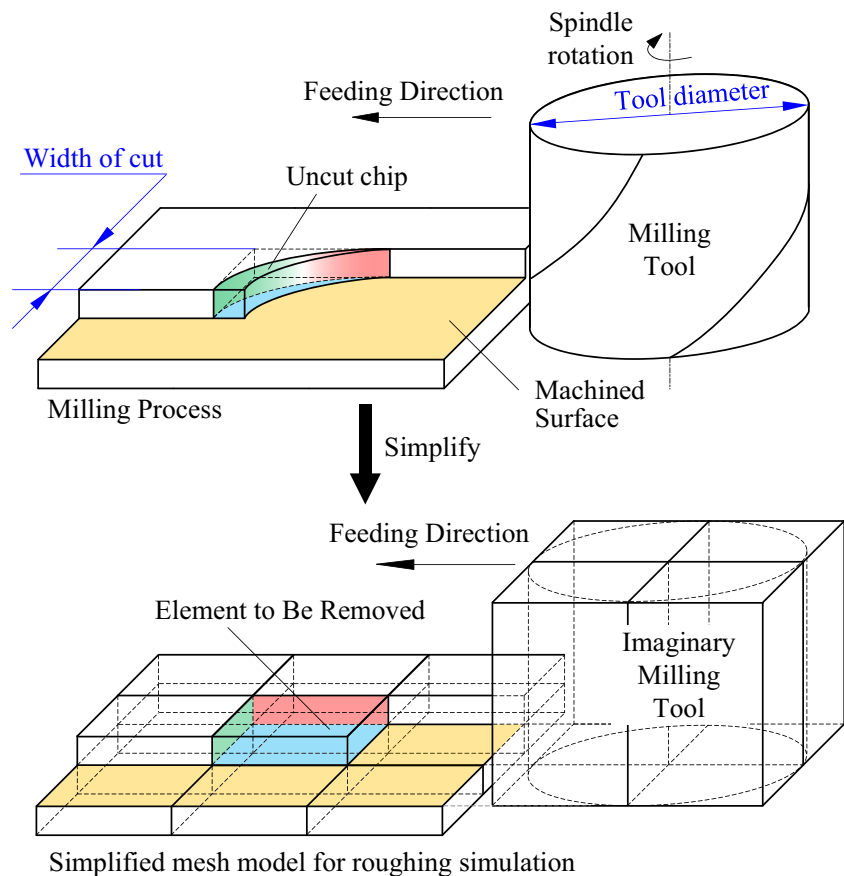
Fig. 3 **a**–**h** Loading cases of cutting forces

workblank; (2) loading of clamping forces; (3) element killing operation (following certain sequence according to the actual

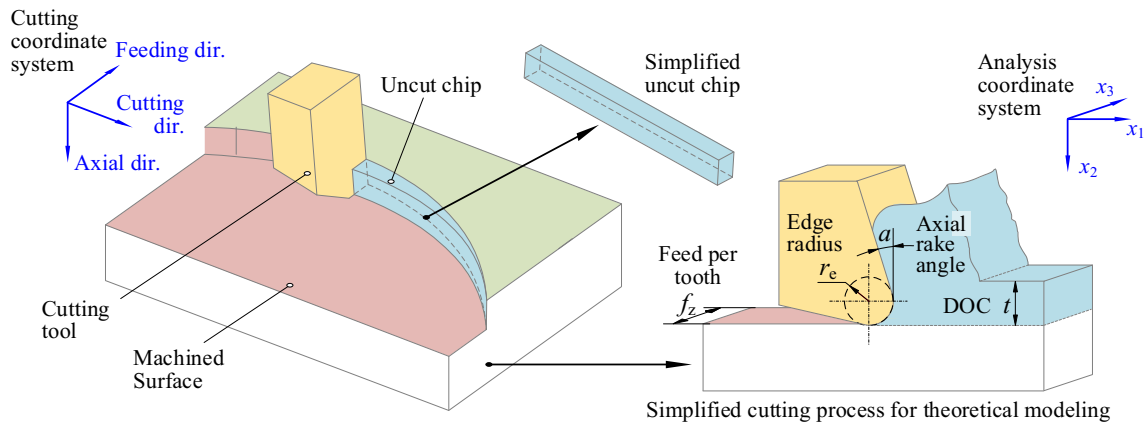tool path); and (4) loading of cutting forces on certain nodes according to the actual tool path.



Fig. 4 Simplified calculation method for MIRS

2.3 Modeling method of the finishing process

For simulation of finishing, a FEM model of the final machined part needs to be built and meshed. This is called the finishing model (FM) in this paper. The size of elements along the depth direction near the machined surface should be small enough (normally in $10^0 \sim 10^1$ μm) to represent the distribution gradient of the MIRS. In this paper, this part of FM with small elements is defined as fine mesh layer. The thickness of fine mesh layer

should be larger than the penetration depth of MIRS (normally in 10^2 μm). The coordinates and stress state of each node in RM, as well as the coordinates of nodes and connectivity data of elements in FM, are output from ABAQUS under the control of Python program. A fitting calculation is needed to map the stress distribution from RM to FM.

The simplified methodology for the analysis of MIRS in the web is shown in Fig. 4. The non-uniform uncut chip in face milling is simplified as uniform, which is a simplification

Fig. 5 Flow chart for MIRS after finishing (partially based on Su et al. [28])
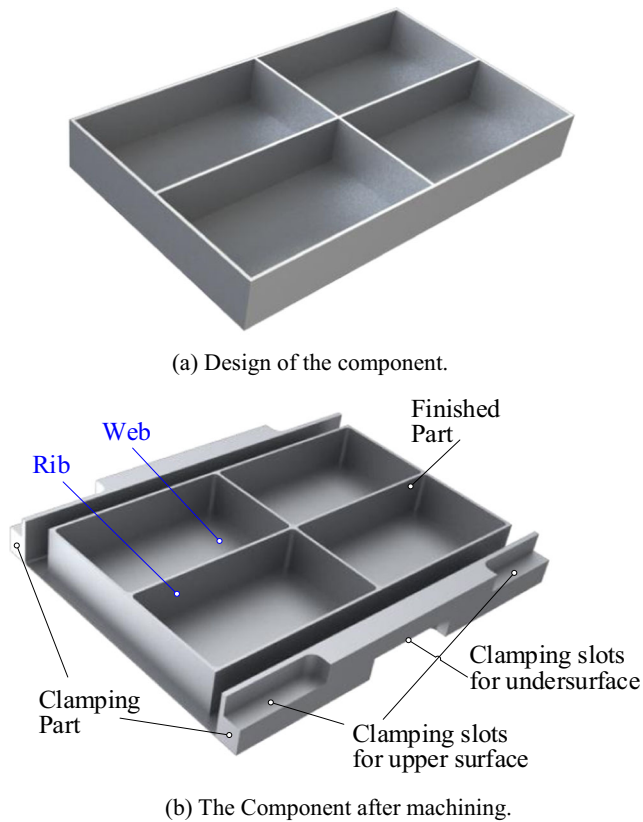
(a) Design of the component.

(b) The Component after machining.
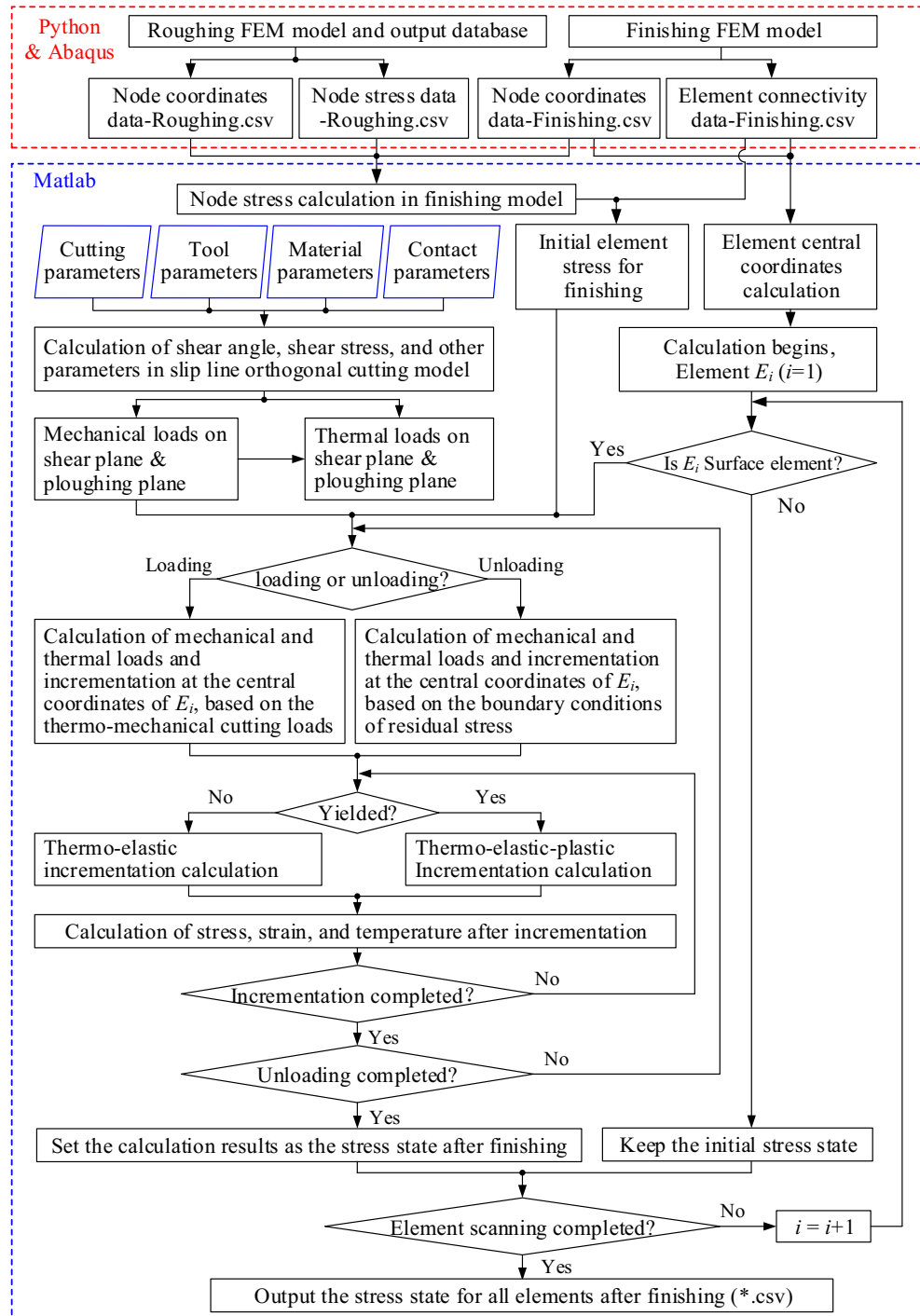
Fig. 6 Designed specimen for machining experiment and simulation. **a** Design of the component, **b** the component after machining

frequently used in FEM simulation of the milling process [26]. The end milling process can be simplified and analyzed with a 2D cutting model [27–29]. The axes x_1, x_2, and x_3 represent the cutting direction, axial direction, and feeding direction, respectively. Subsequently, the residual stress state can be calculated. A similar simplification method for the flank milling process can be found in Su et al. [28].

The theoretical modeling strategy of residual stress calculation for FM is shown in Fig. 5. For each element in FM, the coordinates of its central point are calculated, and its distance to the surface is evaluated. If the element is in the fine mesh layer, i.e., the element is near the machined surface, its stress state after finishing process is calculated with the residual stress model proposed by Su et al. [28]. It is worthy of notice that in theoretical calculations, the thermo-elasto-plastic increment operation starts from the stress state after roughing process rather than zero stress state. If the element is not in the fine mesh layer, i.e., the element would not be plastically influenced by the thermomechanical cutting loads in finishing process, the stress

state of the element would remain the value after roughing. Cutting fluid is usually used during the machining process. According to Ma's analysis [30], a temperature attenuation coefficient of 0.5 should be used in calculation of temperature at the shear plane and the tool-workpiece contact surface, which can approximately represent the influence of cutting fluid on MIRS. MATLAB was used to implement the model.

2.4 Simulation of final residual stress and machining distortion

Residual stress is the self-equilibrating "locked in" stresses that exist in materials without external loads [31]. Thus, the stress distribution after roughing and finishing simulation (with restrictions unreleased) is just an intermediate state. And a stress relaxation process is required to release the internal stress field to reach a self-equilibrating state. During this process, the machining distortion gradually occurs and reaches a steady state.

The calculated stress state can be loaded into the FM as a predefined stress field in ABAQUS. Then, the stress release process can be simulated with a static analysis step in ABAQUS. This allowed the final residual stress distribution and machining distortion to be calculated.

3 Application case of the simulation method

3.1 Design of the component and experiment

A thin-walled component is designed, as shown in Fig. 6a. The dimensions of the component are 393 × 233 × 49 mm. The thicknesses of ribs and webs are 3 mm. The workblank is pre-stretched 7050-T7451 aluminum alloy with dimensions 415 × 325 × 50 mm. The workblank is clamped onto the worktable with four clamping plates. Clamping slots are cut on the workblank to avoid collision. Machining of the component was performed using a DMG DMU 60 monoBLOCK machining center.

The physical properties of 7050-T7451 are listed in Table 1. The coefficients of its Johnson-Cook constitutive equation are shown in Table 2 [32].

The initial residual stress within the workblank was measured with crack compliance method. The measurement specimens (S1 and S2) and the workblank were cut from the same pre-stretched aluminum alloy plate, as shown in Fig. 7a. The

Table 1 Physical properties of 7050-T7451 aluminum alloy

Density [kg/m³]	Thermal conductivity [W/(m K)]	Thermal expansion coefficient [°C⁻¹]	Specific heat [J/(kg °C)]	Young's Modulus [Pa]	Poisson's ratio
2830	157	2.35×10^{-5}	860	7.03×10^{10}	0.33

Table 2 Johnson-Cook coefficients of 7050-T7451 [32]

A [MPa]	B [MPa]	C	n	m	$\dot{\varepsilon}_0$ [s^{-1}]	T_r [°C]	T_{melt} [°C]
463.4	319.5	0.027	0.32	0.99	1	25	635

data was processed with the software developed by Zhou et al. [33]. The distribution of initial residual stress within the aluminum alloy plate is shown in Fig. 7b.
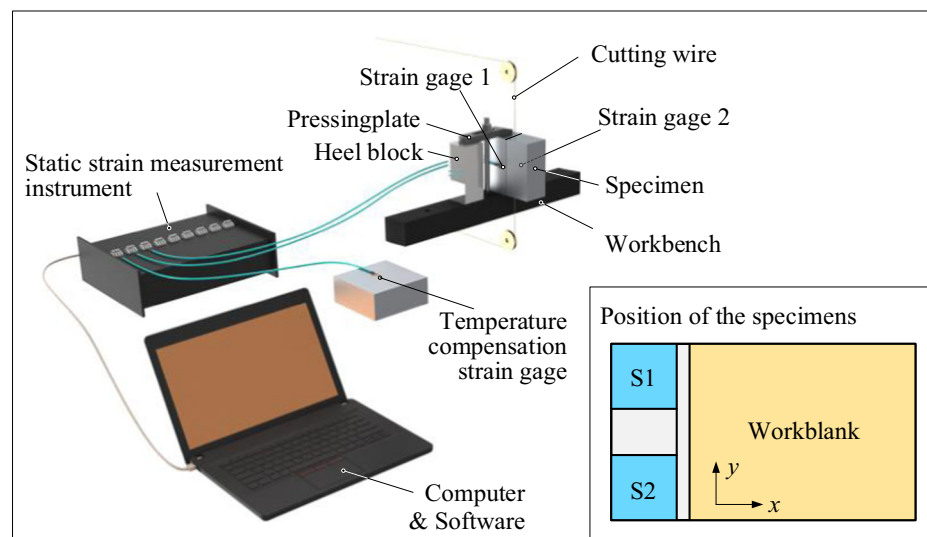
3.2 Machining and measuring experimental setup

Firstly, the clamping slots were machined for the workblank. Then, a facing process was performed on the undersurface using a relatively sharp three-tooth cutting tool (diameter of 10 mm). The spindle speed was 10,000 rpm, the feeding speed was 3000 mm/min, the WOC was 8 mm, and the depth of cut (DOC) was 0.08 mm.

In the roughing process, a three-tooth milling tool, the diameter of which is 20 mm, was used. The DOC was 3 mm. The WOC was 20 mm in the entrance cut and 10 mm in the later cutting process. The roughing of four cavities was performed with a 1 mm machining allowance (tool path shown in Fig. 8). The cutting forces were measured for entrance cut and

Fig. 7 Measurement of initial stress distribution within the workblank. **a** Measurement strategy, **b** measurement results

(a) Measurement strategy.
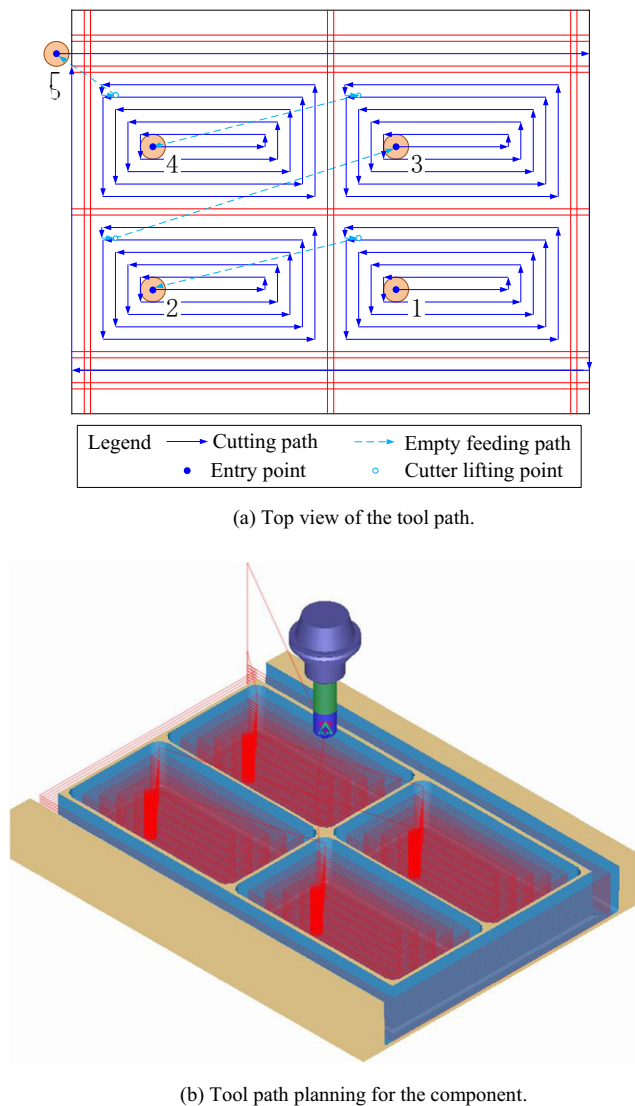

(b) Measurement results.

(a) Top view of the tool path.

(b) Tool path planning for the component.

Fig. 8 Tool path planning for rough machining of the component. **a** Top view of the tool path, **b** tool path planning for the component

After machining, the workpiece was taken off the worktable and the clamping part was removed with bench tools. The component was left to stand to release internal stress and then the profile of the undersurface was measured with a Zeiss CONTURA coordinate measurement machine (CMM).

3.3 Simulation of the roughing process

The RM was built in ABAQUS, as shown in Fig. 9. The dimensions of elements to be removed in roughing are set at $10 \times 10 \times 3$ mm. The size of element along the thickness direction is 1 mm for the thin ribs. Partition operations in ABAQUS are performed to maintain the continuity of the elements. Every element in RM is identified with six indices: [X index of the partition] [Y index of the partition] [Z index of the partition] [local X index of the element] [local Y index of the element] [local Z index of the element].

The element removal sequence was planned according to the tool path. In the simulation of the roughing process, elements in partitions [2][4][1], [2][6][1], [4][4][1], and [4][6][1] were killed in sequence to form the cavities. Next, the elements in partitions [0][8][1], [1][8][1], [2][8][1], [3][8][1], [4][8][1], [5][8][1], [6][8][1], [6][7][1], [6][6][1], [6][5][1], [6][4][1], [6][3][1], [6][2][1], [5][2][1], [4][2][1], [3][2][1], [2][2][1], [1][2][1], [0][2][1], [0][3][1], [0][4][1], [0][5][1], [0][6][1], [0][7][1] were killed in sequence to form the ribs. A total of 1.45×10^4 simulation steps were executed during the roughing simulation in this application case. The simulation requires approximately 8 GB RAM and the output database for a single analysis step is 6–9 GB. This is within the capabilities of mainstream small servers or higher specification personal computers.

The coordinates and stress state of all the remaining nodes were output as *.csv files from the roughing process simulation (using Python scripts), as shown in Fig. 5.

3.4 Simulation of the finishing process

The same machining parameters and layer-by-layer machining technology were used in the machining of the ribs. Consequently, the machining process is approximately symmetrical for both sides of the ribs. Contrastingly, different machining parameters and tool paths were used for the upper and lower surfaces during machining of the web. In this application case, only MIRS on both sides of the web was
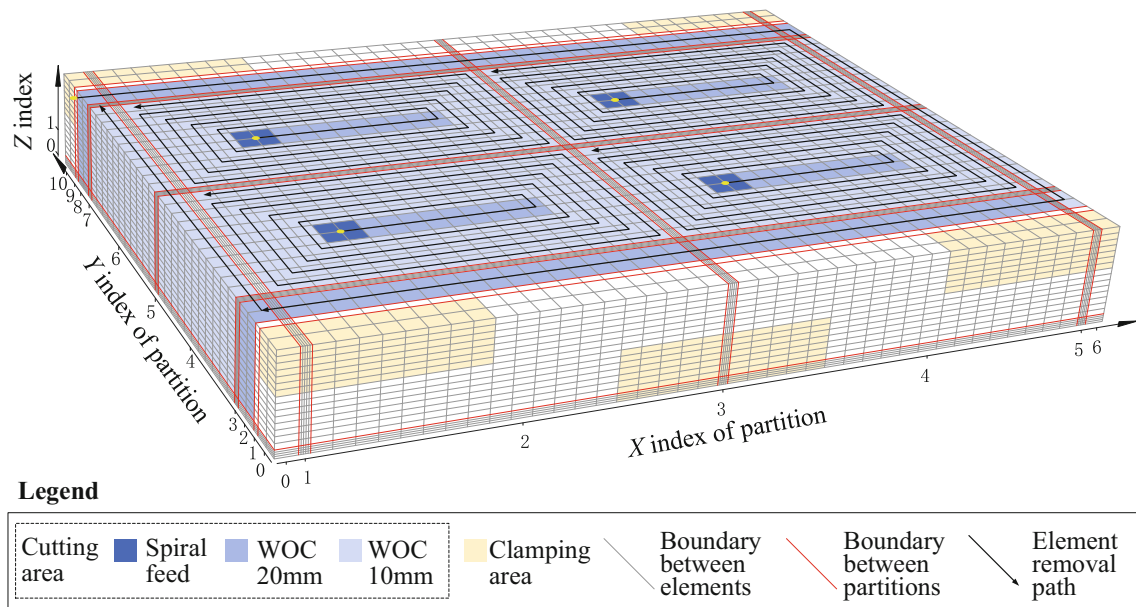
normal cut with a Kistler 9257B dynamometer. The results are shown in Table 3 where F_f, F_p, and F_a are the cutting forces in feeding, peripheral, and axial directions, respectively.

In the finishing process, the spindle speed was 10,000 rpm and the feeding speed was 3000 mm/min. For machining of the ribs, the WOC was 1 mm and the DOC was 2 mm. For machining of the web, the WOC was 8 mm and the DOC was 0.5 mm. The machining was carried out layer by layer to maintain rigidity and reduce local deflection of the thin ribs.

Table 3 Cutting loads in roughing process

Process	Spindle speed [rpm]	Feeding speed [mm/min]	DOC [mm]	WOC [mm]	F_f [N]	F_p [N]	F_a [N]
Entrance cut	10,000	6000	3	20	254.25	443.53	61.34
Normal cut				10	354.40	667.98	119.68

Fig. 9 FEM model for roughing process and element removal planning

considered for the finishing process to limit the scale of theoretical and FEM calculation.

FM was built in the shape of the final component, as shown in Fig. 10. The same meshing strategy with the RM (shown in Fig. 9) was used for the main body of FM to facilitate the mapping of residual stress fields from RM to FM. The meshes were refined within 250 μm of the upper and lower surfaces of the web and the length of element along the normal direction of the surface, d, was set to 10 μm. Next, the coordinate

information of all nodes and the connectivity information of all elements were output in *.csv files.

The residual stress state after the finishing process was calculated for each element in the refined mesh area (following the procedure shown in Fig. 5). The calculation is based on the coordinates of the central point of each element. The simulation strategy for the finishing process is shown in Fig. 11. X and Y represent the global coordinate system of the workpiece. x_1 and x_3 represent the local
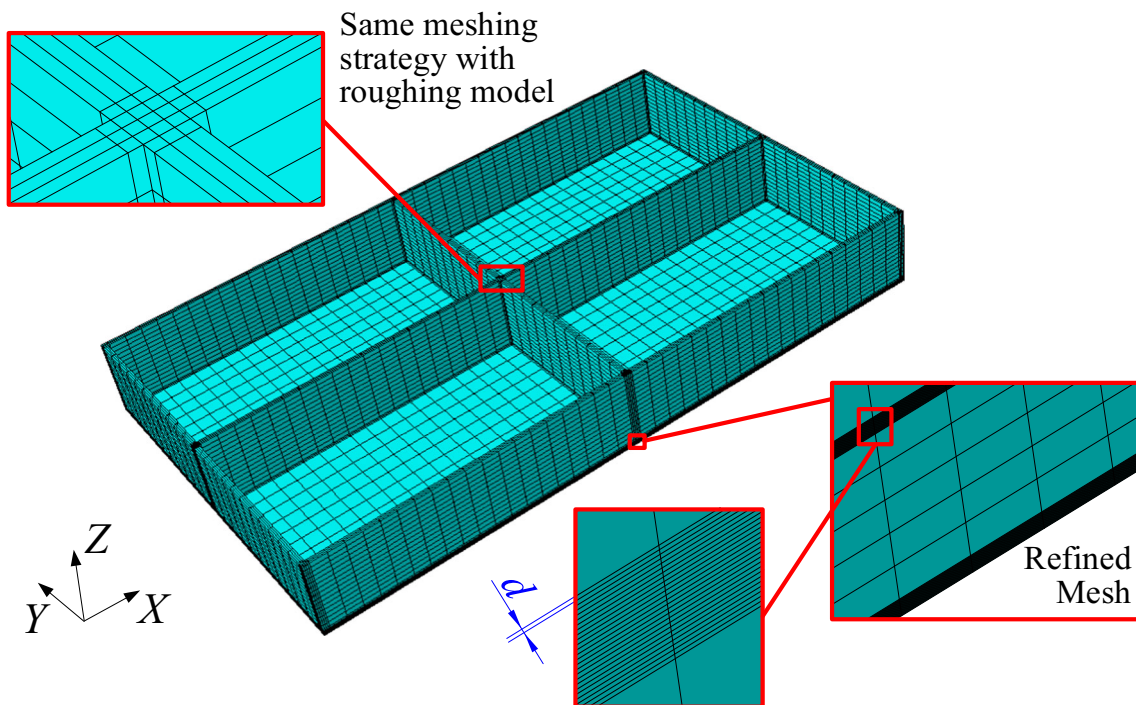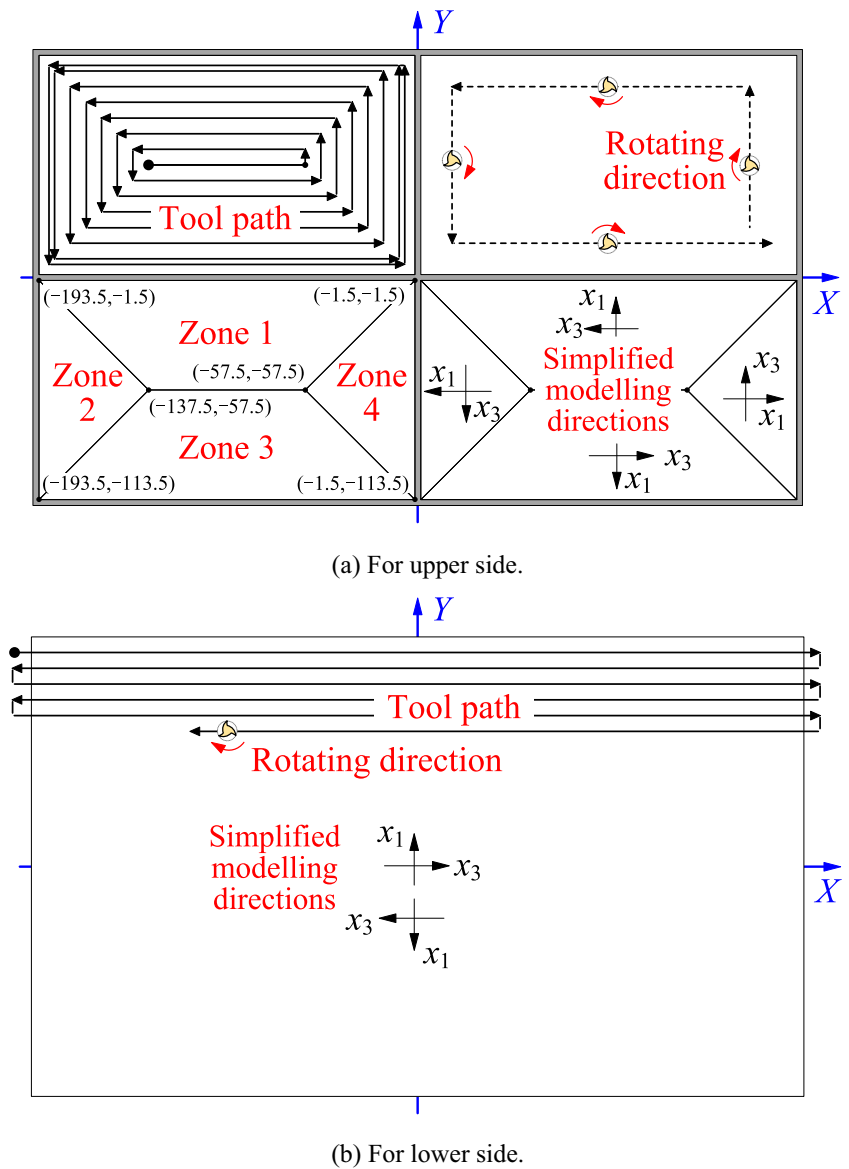

**Fig. 10** Finite element model of the completed component

Fig. 11 Simulation strategy for the finishing process. **a** For upper surface of the web, **b** for lower surface of the web

(a) For upper side.

(b) For lower side.

coordinate system used for the residual stress calculation in accordance with the analysis model shown in Fig. 4.

The calculated data were output in a *.csv file. Next, an analysis step in ABAQUS was performed to calculate the

Fig. 12 Profile of undersurface measured by CMM
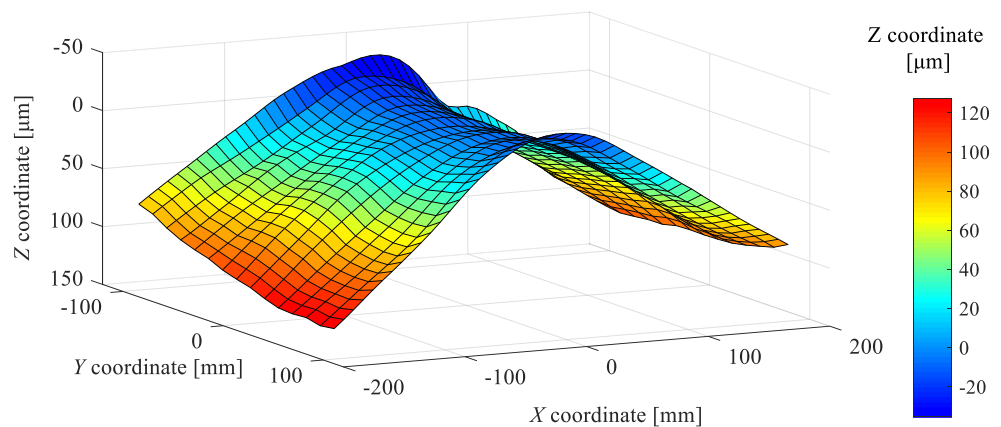
final distortion of the workpiece (using the *.csv file to set the predefined stress state).

A reference case neglecting MIRS was also calculated, which represents the conventional method for distortion simulation of the thin-walled parts. In the reference case, the stress state after roughing simulation was used directly to simulate final distortion.

4 Results of experiment and simulation

4.1 Machining distortion of the workpiece

The measured profile of the undersurface is shown in Fig. 12. The deformation along X direction is convex. The deformation along Y direction is concave. The deformation along X direction forms the main deformation of the undersurface. Overall, the undersurface is saddle-shaped and the distortion is approximately X and Y symmetric. The planeness error is 175.2 μm.

## 4.2 FEM simulation results for the roughing process

Using the measured stress distribution of the aluminum alloy plate (shown in Fig. 7b), the stress state of each element in the RM was calculated according to the Z coordinate of its center. These stress data were loaded into ABAQUS as predefined stress field, as shown in Fig. 13a. The balanced internal stress distribution is shown in Fig. 13b. There is little change in stress distribution within most inner part of the workblank. However, the stress distribution near the boundary area changes remarkably.

The internal stress field of the workpiece evolves with the removal of work material, as shown in Fig. 14. The elements in four cavities are removed cavity by cavity. During this process, the internal stress field is inhomogeneous and asymmetric. The internal stress field shows symmetry on completion of the roughing simulation. This is because of the symmetric initial stress distribution and symmetric structure. Mechanical loads can influence the local stress distribution near the cutting zone. However, this local effect has little influence on the final stress field.

Fig. 13 Distribution of internal stress within workblank (normal stress in X direction). **a** Predefined internal stress state, **b** balanced internal stress state
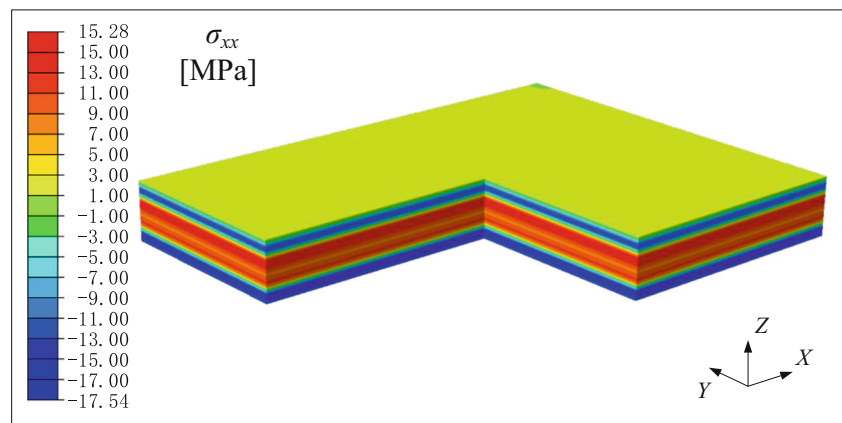
(a) Predefined internal stress state.
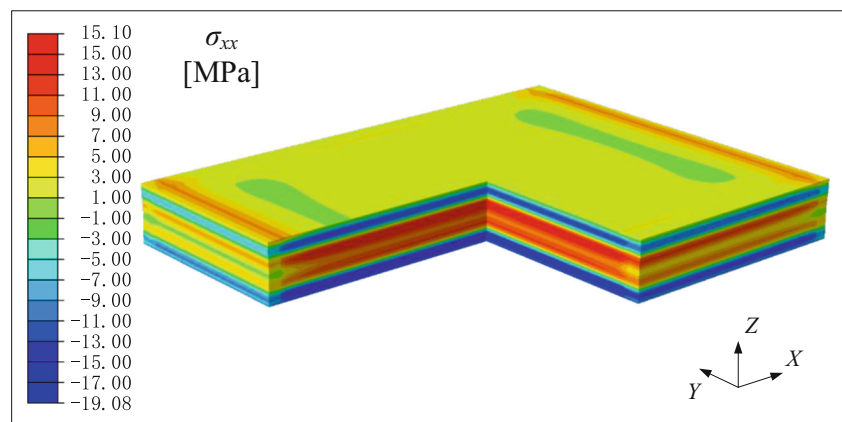
(b) Balanced internal stress state.

4.3 Simulation of the finishing process and the final distortion

After the roughing simulation, the stress field was output from RM and mapped to FM (shown in Fig. 15).

The stress state for every element in the upper and lower surface (up to 250 μm depth) of the web is calculated according to its position and its stress state after roughing, following the flow chart shown in Fig. 5. As

a reference, the calculated stress distribution with zero initial stress is shown in Fig. 16.

The simulated machining distortion profiles are shown in Fig. 17. In this study, the simulated profiles of the undersurfaces for both calculation cases are convex. The simulated profile along the X direction at the central area shows the main distortion trend and agrees with experimental results. Considering the simulation accuracy of planeness, the more comprehensive
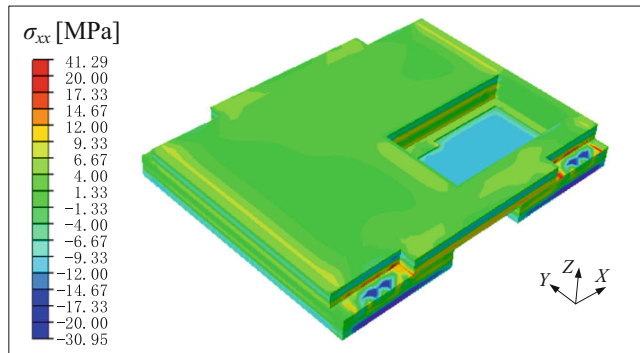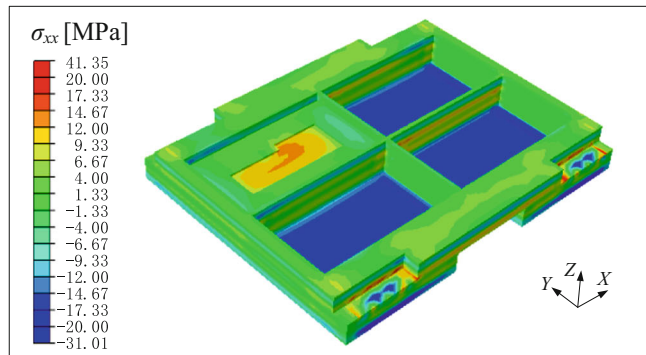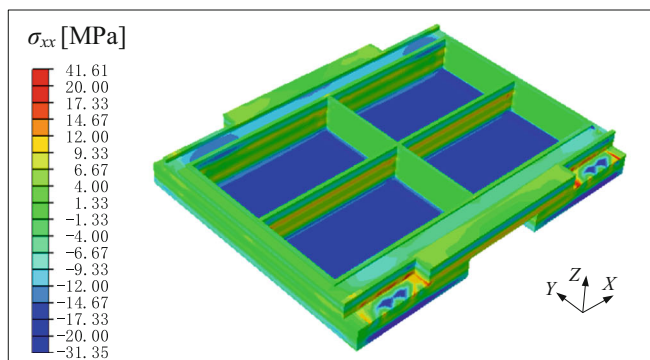

(a) Stress field after 2500 analysis steps.
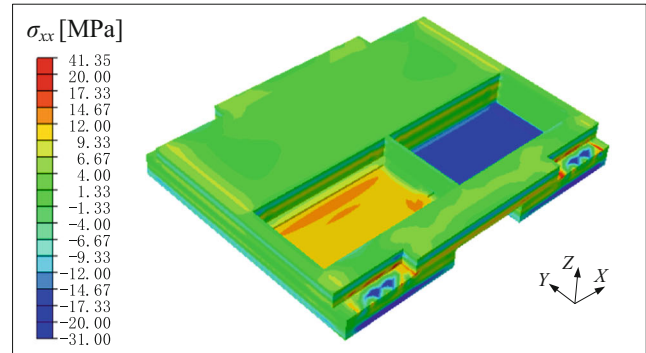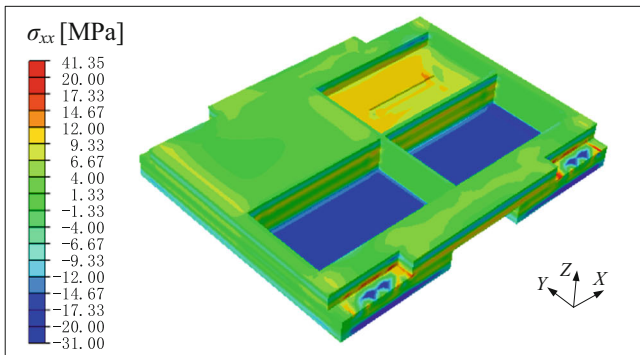
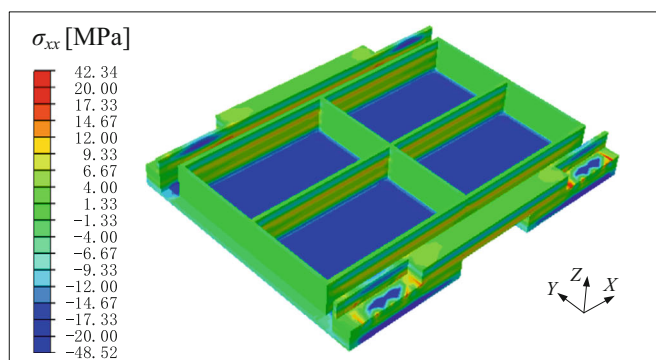(b) Stress field after 4900analysis steps.

(c) Stress field after 7300 analysis steps.

(d) Stress field after 9700 analysis steps.

(e) Stress field after 12100 analysis steps.

(f) Stress field after 14500 analysis steps.

Fig. 14 Representative simulation results for the roughing process (normal stress in X direction). **a** Stress field after 2500 analysis steps, **b** stress field after 4900 analysis steps, **c** stress field after 7300 analysis steps, **d** stress field after 9700 analysis steps, **e** stress field after 12,100 analysis steps, **f** stress field after 14,500 analysis steps
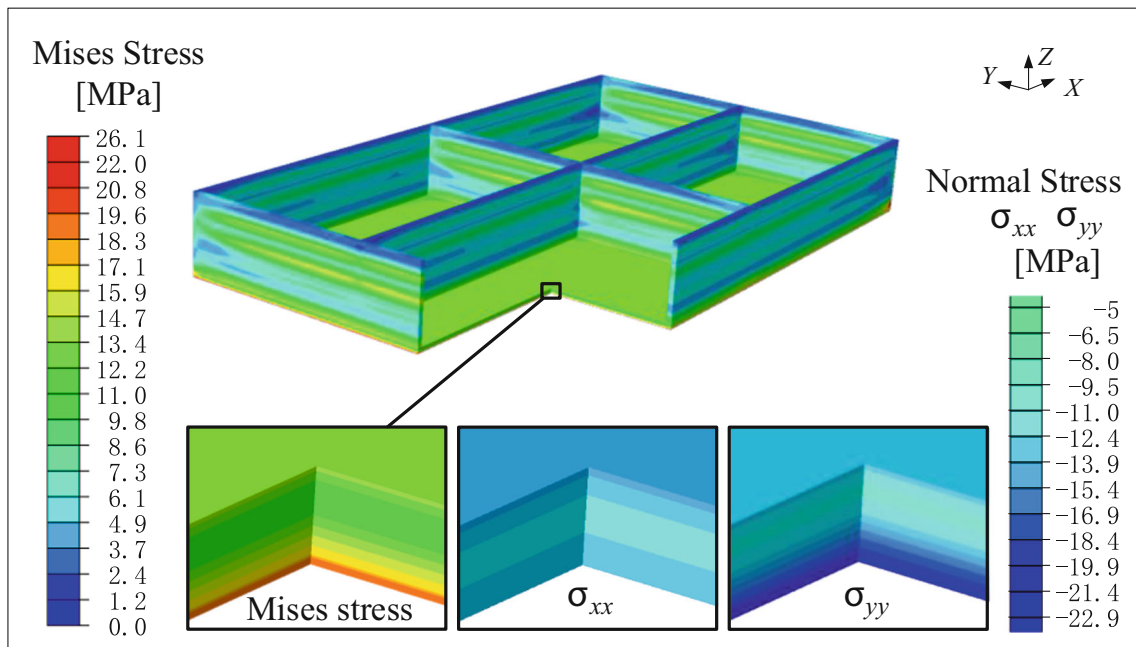
**Fig. 15** Mapping results of the stress field (from RM to FM)

calculation case that considers MIRS achieves significantly better accuracy with relative error of approximately 17%. The calculation case ignoring MIRS within the machined surface has relative error of approximately 37%.

5 Discussion

5.1 On the proposed combined method

An analysis method for part-level machining distortion is proposed. It combines FEM and theoretical calculation. FEM can analyze the evolution of the stress field and distortion for complicated structures. It can achieve good calculation efficiency and accuracy within the linear-elastic range. Simulation of the metal machining process with FEM is time consuming and is not practical for part-level simulation. In contrast, theoretical analysis can achieve good calculation efficiency in modeling MIRS. A combination of these two methods can be used to reproduce the internal stress evolution process due to mass material removal and machining loads. This is a practical approach for part-level machining simulation and distortion control (especially for large-scale and thin-walled components). The new combined method proposed in this paper showed better accuracy in predicting the planeness
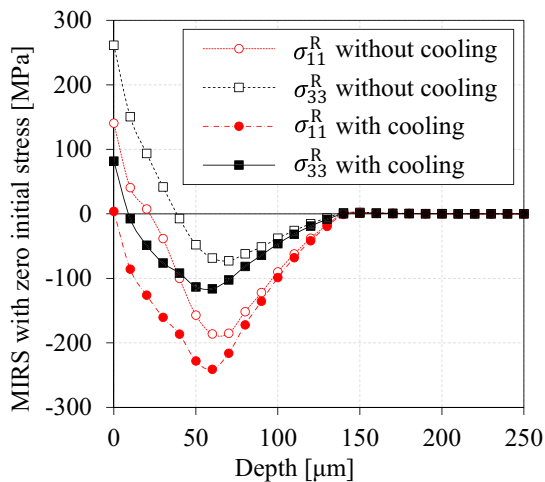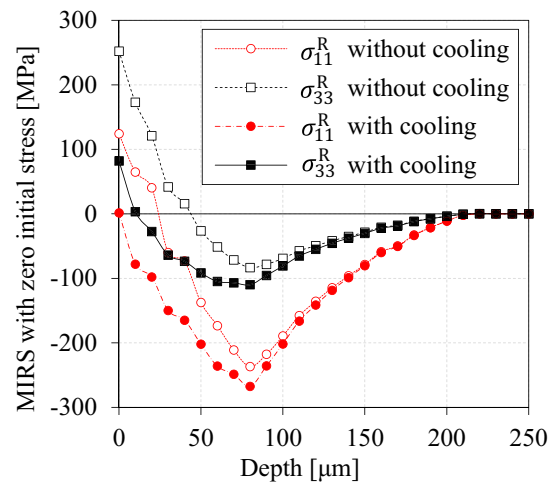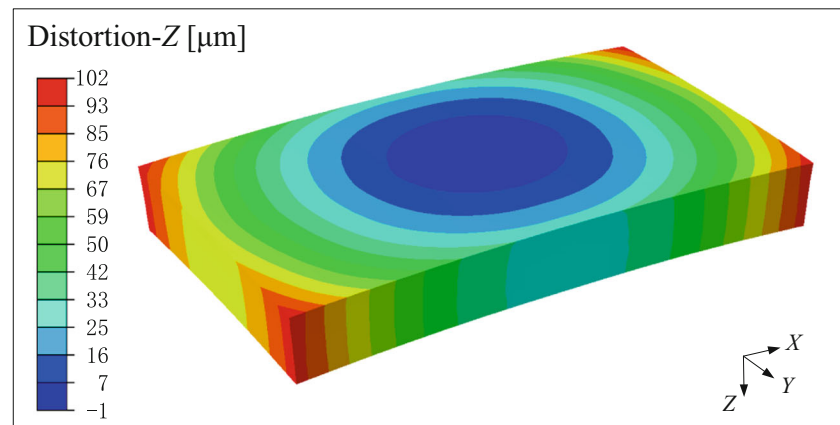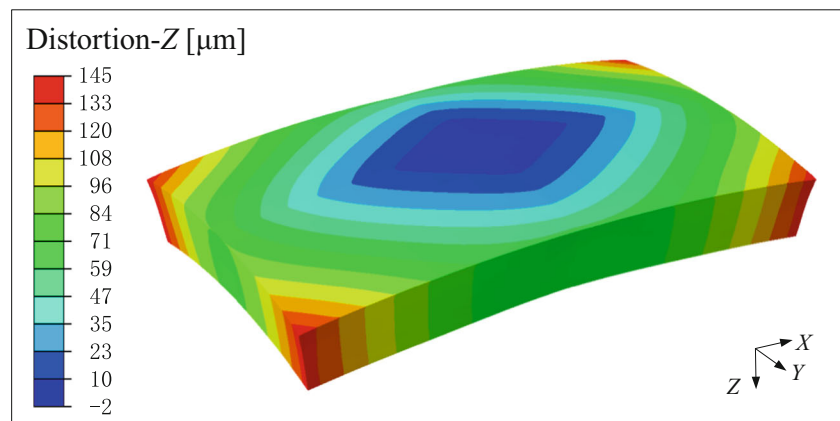

(a) For upper surface of the web.   (b) For lower surface of the web.

Fig. 16 Calculated MIRS distribution after finishing (without initial stress). **a** For upper surface of the web, **b** for lower surface of the web

Fig. 17 Simulated final distortion after machining. **a** Simulation ignoring MIRS, **b** simulation considering MIRS

Distortion-Z [μm]

(a) Simulation ignoring MIRS.

Distortion-Z [μm]

(b) Simulation considering MIRS.

error for the application considered. The results also indicate that the redistribution of workblank residual stress is the main source of machining distortion of the aluminum alloy thin-walled components, which is in accordance with the research of Yang et al. [34]. Finally, it is shown that the influence of MIRS should not be neglected in simulations.

5.2 Simulation errors

The two main sources of error when applying this method are discussed below:

(1)   The error in measuring initial residual stress within the workblank.

The crack compliance method was used to measure residual stress distribution within the workblank. One important assumption of this method is that the residual stress only varies along thickness direction. However, this is not workable at the border region of the aluminum plate. The length and width of the test specimen is usually only 2−2.5 times its thickness for the

measurement of residual stress in the aluminum plate. The non-uniform distribution of residual stress near the border may influence the measuring accuracy. However, this influence has not been fully studied.

The redistribution of residual stress within the workblank is the main source of machining distortion. Hence, the accuracy of the initial stress input is of crucial importance to the overall analysis accuracy. The overall simulation accuracy of machining distortion might be further improved by either better measuring technology that can scan the 3D stress distribution within material, or by a complete FEM analysis of the forming and pre-processing of the workblank.

(2)   The error in theoretical modeling of machining-induced residual stress.

2D analysis for MIRS was used to model the internal stress evolution during the finishing process. The 2D simulation cannot fully reveal the 3D stress and temperature field in the milling process, which may cause errors. To the author's knowledge, there is still no mature 3D theoretical modeling technology for the machining process and MIRS because of

the complexity of the process. Further research is required on this issue in the future.

A further challenge is to comprehensively understand and model the material behavior during the machining process. This involves non-uniform deformation with large strain, high strain rate, and high temperature. The constitutive model and many physical parameters of the material all vary under different conditions. At present, a simplified model and/or constant values must be selected for theoretical modeling and FEM analysis. Increased simulation accuracy depends largely on the improvement of the material model.

6 Summary

A new simulation method for part-level machining distortion is presented and applied to a test case. The following conclusions were drawn:

(a) The combined FEM analysis and theoretical modeling simulation method can be used to track the evolution of the internal stress field during the machining process. The method can be implemented on current mainstream small servers or higher specification personal computers.

(b) The evolution of initial stress within the workblank due to material removal is the main cause of machining distortion for thin-walled components, while MIRS cannot be neglected in simulations.

(c) The material removal process and cutting loads must be accounted for to accurately predict machining distortion. In FEM analysis, the meshes should be configured to represent the distribution gradient of stress.

Compliance with ethical standards

Conflict of interest The authors declare that they have no conflict of interest.

References

1. Sim WM (2010) Challenges of residual stress and part distortion in the civil airframe industry. Int J Microstruct Mater Prop 5:446–455. https://doi.org/10.1504/ijmmp.2010.037621

2. Guo H, Zuo DW, Wu HB, Xu F, Tong GQ (2009) Prediction on milling distortion for aero-multi-frame parts. Mater Sci Eng A 499: 230–233. https://doi.org/10.1016/j.msea.2007.11.137

3. Li JG, Wang SQ (2017) Distortion caused by residual stresses in machining aeronautical aluminum alloy parts: recent advances. Int J Adv Manuf Technol 89:997–1012. https://doi.org/10.1007/s00170-016-9066-6

4. Garcia DR, Hill MR, Aurich JC, Linke BS (2017) Characterization of machining distortion due to residual stresses in quenched aluminum. ASME 2017 12th International Manufacturing Science and Engineering Conference, Los Angeles

5. Wang QC (2003) Evaluation and relief of residual stresses in aluminum alloys for aircraft structures. Dissertation, Zhejiang University

6. Robinson JS, Tanner DA, Truman CE, Wimpory RC (2011) Measurement and prediction of machining induced redistribution of residual stress in the aluminum alloy 7449. Exp Mech 51:981–993. https://doi.org/10.1007/s11340-010-9389-4

7. Guo H (2005) Study on mechanism and prediction analysis of machining distortion for aero-multi-frame monolithic structure. Dissertation, Nanjing University of Aeronautics and Astronautics

8. Rai JK, Xirouchakis P (2008) Finite element method based machining simulation environment for analyzing part errors induced during milling of thin-walled components. Int J Mach Tools Manuf 48: 629–643. https://doi.org/10.1016/j.ijmachtools.2007.11.004

9. Sasahara H (2005) The effect on fatigue life of residual stress and surface hardness resulting from different cutting conditions of 0.45%C steel. Int J Mach Tools Manuf 45:131–136. https://doi.org/10.1016/j.ijmachtools.2004.08.002

10. Wan Y, Cheng K, Fu XL, Liu ZQ (2013) An experiment-based investigation on surface corrosion resistance behaviors of aluminum alloy 7050-T7451 after end milling. P I Mech Eng C-J MEC 227:1297–1305. https://doi.org/10.1177/1350650113491084

11. Masoudi S, Amini S, Saeidi E, Eslami-Chalander H (2015) Effect of machining-induced residual stress on the distortion of thin-walled parts. Int J Adv Manuf Technol 76:597–608. https://doi.org/10.1007/s00170-014-6281-x

12. Young KA (2005) Machining-induced residual stress and distortion of thin parts. Dissertation, Washington University

13. Huang X, Sun J, Li J (2015) Finite element simulation and experimental investigation on the residual stress-related monolithic component deformation. Int J Adv Manuf Technol 77:1035–1041. https://doi.org/10.1007/s00170-014-6533-9

14. Ma Y, Yu DW, Feng PF, Wu ZJ, Zhang JF (2015) Finite element method study on the influence of initial stress on machining process. Adv Mech Eng 7:168781401557245. https://doi.org/10.1177/1687814015572457

15. Mabrouki T, Girardin FO, Asad M, Rigal JO (2008) Numerical and experimental study of dry cutting for an aeronautic aluminium alloy (A2024-T351). Int J Mach Tools Manuf 48:1187–1197. https://doi.org/10.1016/j.ijmachtools.2008.03.013

16. Jiang XH, Li BZ, Yang jG, Zuo XY (2013) Effects of tool diameters on the residual stress and distortion induced by milling of thin-walled part. Int J Adv Manuf Technol 68:175–186. https://doi.org/10.1007/s00170-012-4717-8

17. Yao CF, Wu DX, Tan L, Ren JX, Shi KN, Yang ZC (2013) Effects of cutting parameters on surface residual stress and its mechanism in high-speed milling of TB6. Proc Inst Mech Eng B J Eng Manuf 227:483–493. https://doi.org/10.1177/0954405413475771

18. Liang SY, Su JC (2007) Residual stress modeling in orthogonal machining. CIRP Ann Manuf Technol 56:65–68. https://doi.org/10.1016/j.cirp.2007.05.018

19. Su J, Young KA, Srivatsa S, Morehouse JB, Liang SY (2013) Predictive modeling of machining residual stresses considering tool edge effects. Prod Eng 7:391–400. https://doi.org/10.1007/s11740-013-0470-6

20. Huang X, Zhang X, Ding H (2016) A novel relaxation-free analytical method for prediction of residual stress induced by mechanical

load during orthogonal machining. Int J Mech Sci 115-116:299–309. https://doi.org/10.1016/j.ijmecsci.2016.06.024

21. Huang K, Yang W (2016) Analytical modeling of residual stress formation in workpiece material due to cutting. Int J Mech Sci 114:21–34. https://doi.org/10.1016/j.ijmecsci.2016.04.018

22. Fergani O, Jiang X, Shao Y, Welo T, Yang J, Liang S (2016) Prediction of residual stress regeneration in multi-pass milling. Int J Adv Manuf Technol 83:1153–1160. https://doi.org/10.1007/s00170-015-7464-9

23. Prime MB (1999) Residual stress measurement by successive extension of a slot: the crack compliance method. Appl Mech Rev 52:75–96. https://doi.org/10.1115/1.3098926

24. Joun MS, Lee MC, Park JM (2002) Finite element analysis of prestressed die set in cold forging. Int J Mach Tools Manuf 42:1213–1222. https://doi.org/10.1016/S0890-6955(02)00079-2

25. Chobaut N, Wagner JN, Carron D, Saelzle P, Pirling T, Hofmann M, Drezet JM (2017) Stress generation during the quenching of large AA2618 forgings: finite element computations and validation against neutron diffraction measurements. Finite Elem Anal Des 131:17–24. https://doi.org/10.1016/j.finel.2017.03.004

26. Huang ZG, Ke YL, Dong HY (2005) Finite element model of milling process sequence for frame monolithic components. Journal of Zhejiang University (Engineering Science) 39:368–372. https://doi.org/10.3785/j.issn.1008-973X.2005.03.012

27. Ma Y, Feng PF, Zhang JF, Wu ZJ, Yu DW (2015) Energy criteria for machining-induced residual stresses in face milling and their relation with cutting power. Int J Adv Manuf Technol 81:1023–1032. https://doi.org/10.1007/s00170-015-7278-9

28. Su JC, Young KA, Ma K, Srivatsa S, Morehouse JB, Liang SY (2013) Modeling of residual stresses in milling. Int J Adv Manuf Technol 65:717–733. https://doi.org/10.1007/s00170-012-4211-3

29. Su JC (2006) Residual stress modeling in machining processes. Dissertation, Georgia Institute of Technology

30. Ma Y (2016) Evolution mechanism of machining-induced residual stress and its influence on machining distortion of thin-walled components. Dissertation, Tsinghua University

31. Schajer GS, Ruud CO (2013) Overview of residual stresses and their measurement. In: Schajer GS (ed) Practical residual stress measurement methods. Wiley, pp 1–27

32. Fu XL (2007) Research on deformation theory and characteristics of machined surface for high-speed milling aviation aluminum alloy. Dissertation, Shandong University

33. Zhou CA, Sun J, Li WD, Wang W (2014) The measurement of original residual stress in aircraft aluminum alloy. Mechanical Science and Technology for Aerospace Engineering 33:1251–1254. https://doi.org/10.13433/j.cnki.1003-8728.2014.0828

34. Yang Y, Li M, Li KR (2014) Comparison and analysis of main effect elements of machining distortion for aluminum alloy and titanium alloy aircraft monolithic component. Int J Adv Manuf Technol 70:1803–1811. https://doi.org/10.1007/s00170-013-5431-x